Phys. Status Solidi RRL **7**, No. 10, 815–830 (2013) / **DOI** 10.1002/pssr.201307109

Part of Focus Issue on
Semiconductor Nanowires
Eds.: Chennupati Jagadish, Lutz Geelhaar, Silvija Gradecak

pss +++rapid research letters+++
www.pss-rapid.com

Review@RRL

III–V nanowire photovoltaics: Review of design for high efficiency

R. R. LaPierre*, A. C. E. Chia, S. J. Gibson, C. M. Haapamaki, J. Boulanger, R. Yee, P. Kuyanov, J. Zhang, N. Tajik, N. Jewell, and K. M. A. Rahman

Department of Engineering Physics, McMaster University, 1280 Main St. West, Hamilton, Ontario, L8S 4L7, Canada

Received 12 March 2013, revised 4 April 2013, accepted 4 April 2013
Published online 11 April 2013

Keywords nanowires, photovoltaics, solar cells, III–V semiconductors

* Corresponding author: e-mail lapierr@mcmaster.ca, Phone: +01 905 525 9140, Fax: +01 905 527 8409

This article reviews recent developments in nanowire-based photovoltaics (PV) with an emphasis on III–V semiconductors including growth mechanisms, device fabrication and performance results. We first review the available nanowire growth methods followed by control of nanowire growth direction and crystal structure. Important device issues are reviewed, including optical absorption, carrier collection, strain accommodation, design for high efficiency, tunnel junctions, Ohmic contact formation, passivation and doping. Performance data of III–V nanowire cells and the primary challenges in nanowire PV are summarized. Many of the issues discussed here are also applicable to other nanowire devices such as photodetectors.

1 Introduction Global energy demand is predicted to exceed 30 TW by 2050, about double the present value [1]. This predicament, known as the TeraWatt challenge, and concern over anthropogenic climate change, resource availability ("peak energy") and energy security have all increased the interest in renewable energy (hydroelectric, wind, solar, geothermal and biomass) [2]. One of the most promising renewable energy technologies is solar photovoltaics (PV) which convert sunlight directly into electrical energy. Although the resource potential of PV is enormous, it currently constitutes a small fraction (<1%) of global energy supply [2]. One of the main factors limiting the widespread adoption of PV is its low energy density, low efficiency, and relatively high cost in comparison to other energy technologies. This means that current PV technology can only compete in areas of high insolation or by government incentives such as feed-in tariff programs.

One of the most relevant metrics for PV devices is the power conversion efficiency (PCE); that is, the efficiency with which sunlight can be converted to electrical power. A significant effort in PV research today aims to improve PCE while simultaneously reducing (or, at least, not significantly impacting) production cost. The vast majority of today's PV market consists of first generation technology defined as single p–n junctions formed in single crystal Si substrates or, more commonly now, multi-crystalline Si substrates. Second generation PV, also known as thin film PV, aims to reduce cost by utilizing less material, and depositing on inexpensive substrates such as metal foil, glass and plastic. These include amorphous Si, cadmium telluride (CdTe) and copper indium gallium diselenide (CIGS), all of lower material quality and PCE compared to first generation cells. To overcome these limitations, third generation solar cells [3] are currently being pursued that aim to overcome the Shockley–Queisser efficiency limit [4] of ~30% (1 Sun) for a single p–n junction, while maintaining or reducing cost. The highest efficiencies in this category are achieved by III–V cells that employ highly perfect thin films of Group III–V compound semiconductor materials in a multi-junction device structure, which consists of tandem sub-cells connected electrically in series [5]. By absorbing a wider wavelength range within a number of subcells, these multi-junction solar cells have achieved the highest efficiencies of any PV technology with a current record of 44% under concentrated sunlight (942 Suns) [6]. However, the materials and fabrication for III–V multi-

junction cells are very expensive (>$10 per cm^2 of cell area). Therefore, this technology is deployed terrestrially in concentrator systems which typically reduce the cell area required by a factor of several hundred, replacing the high cost of the cell with the low cost of focusing optics (lenses or mirrors) [7].

To overcome the limitations of current III–V multijunction cells, III–V nanowire-based solar cells are being aggressively pursued by numerous groups. Nanowire-based solar cells replace the traditional optical absorber (planar substrate or thin film) with a "forest" of one-dimensional rods, wires, or pillars having lengths typically on the order of microns and diameters on the order of tens to hundreds of nanometers. Throughout this review, we refer to these structures as nanowires, although the terms "nanorods", "nanopillars" and "whiskers" have also been used in the literature. In subsequent sections, we will highlight the advantages of nanowire-based structures compared to their planar counterparts to improve PCE, as well as opportunities for significant cost reduction. Issues on control of nanowire parameters are also examined. We focus on the "bottom–up" grown nanowires rather than the top–down methods involving etching since the former method affords greater control and possibilities in device design. Several notable review articles on nanowire PV already exist [8–12]. However, this is a rapidly advancing field and recent developments merit further review.

2 Nanowire growth methods

Three dominant methods exist for III–V nanowire growth: (i) catalyst-assisted growth by molecular beam epitaxy (MBE), metalorganic vapour phase epitaxy (MOVPE), or their variants; (ii) self-catalyzed nanowire growth by MBE, MOVPE, or their variants; and (iii) selective-area growth by MOVPE. Most of the nanowire growth techniques have employed MBE or MOVPE, although their variants such as chemical beam epitaxy (CBE) are also certainly possible. Other techniques, such as laser ablation pioneered by the Lieber group [13], will not be described here.

Ray LaPierre attended Dalhousie University (Halifax, Nova Scotia, Canada) where he obtained a B.Sc. degree in Physics in 1992. He then completed his M. Eng. degree in 1994 and Ph.D. degree in 1997 in the Engineering Physics Department at McMaster University (Hamilton, Ontario, Canada). His graduate work involved development of molecular beam epitaxy of InGaAsP alloys for laser diodes in telecom applications. Upon completion of his graduate work in 1997, he joined JDS Uniphase (Ottawa, Ontario, Canada) where he developed dielectric coatings for wavelength division multiplexing devices. In 2004, he rejoined McMaster University as an Assistant Professor in the Engineering Physics Department. He is currently an Associate Professor and Associate Chair (Graduate Studies) in the Engineering Physics Department with interests in III–V nanowires, molecular beam epitaxy, and applications in photovoltaics, photodetectors and quantum information processing.

2.1 Catalyst-assisted growth The catalyst-assisted nanowire growth method (Fig. 1a), employing a foreign metal particle, is the oldest and most studied of the nanowire growth techniques. A foreign metal seed particle (typically Au; often called the catalyst) acts as a collector for the growth species in an MBE or MOVPE system or their derivatives. Growth species collect in the metal droplet (seed particle) by direct impingement, by diffusion after impingement on the surrounding substrate surface (the collection area), or by diffusion after impingement on the nanowire sidewall surfaces (following initial formation of the nanowire). Supersaturation of the seed particle by the growth species results in the nucleation and epitaxial growth of nanowire material under each seed particle.

This growth mechanism, also known as the vapour–liquid–solid (VLS) method, was first described for Si whiskers by Wagner and Ellis at Bell Laboratories in 1964 [14]. Givargizov later provided a more detailed study of the VLS growth mechanism in Si whiskers by CVD [15]. The VLS method has since been used to grow almost all III–V compound semiconductors including phosphides, arsenides, antimonides and even some ternary alloy compounds. Various methods exist for seed particle formation including thermal evaporation, colloids, or aerosols [16, 17]. Patterned growth can be achieved by standard lithography procedures, such as electron beam lithography (EBL) [18] or nanoimprint lithography (NIL) [19] to produce an Au dot array.

Axial and core–shell (radial, coaxial) heterostructures or dopant profiles, that are essential for most devices, are achieved by switching of growth species during growth. It is believed that group V solubility in the Au droplet is much smaller (on the order of a few at%) compared to group III material, which has implications in the control of heterostructures (discussed further in Section 14). In MBE, the nanowire morphology and the type of heterostructure grown (radial or axial) are determined by the diffusivity of

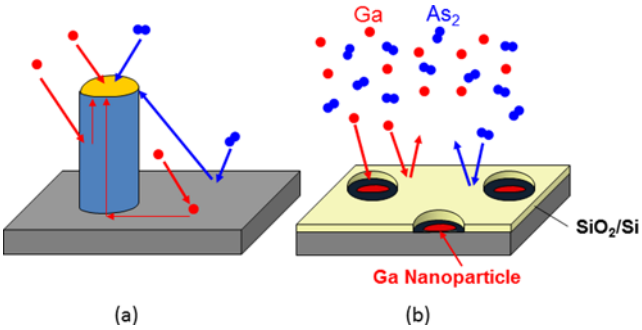

Figure 1 (a) Au-assisted nanowire growth, showing Ga (red) and As_2 (blue) adatoms impinging, diffusing or desorbing toward the Au particle (yellow). (b) Initial stages of Ga-assisted growth of GaAs nanowires, showing Ga droplet formation in SiO_2 holes on a Si substrate.

the growth species which is dictated by growth conditions (temperature, impingement rate, V/III flux ratio) [20–25]. The dominant growth mechanism is believed to be group III diffusion from the nanowire sidewall surfaces [25] with long adatom diffusion lengths favouring axial VLS growth. Conversely, short diffusion lengths favour radial growth by vapour–solid (VS) deposition on the nanowire sidewalls. In MBE, diffusion lengths can be kinetically controlled by growth conditions. In MOVPE, different decomposition rates of the metalorganic precursors on the Au droplet versus the nanowire sidewalls can also influence the nanowire morphology [26]. In addition, the density of Au particles [27], shadowing effects from neighboring nanowires in the case of MBE [28], synergetic effects due to secondary adsorption [29], and competition among neighboring nanowires due to overlapping collection areas may further complicate nanowire growth.

2.2 Self-assisted growth The self-catalyzed or self-assisted growth method (Fig. 1b), performed by MBE or MOVPE (or their variants), is a VLS method that uses a seed particle which is a constituent of the nanowire itself [30–36]; for example, Ga is used as the seed particle for GaAs nanowire growth, or In seed for the growth of InAs or InP nanowires. A review is provided in Ref. [34]. In this process, the substrate surface is covered in an oxide (e.g., a native, thermally grown, or deposited oxide). In MBE, for example, Ga adatoms impinge and form droplets at holes or defects in the native oxide or at intentionally patterned holes (e.g., holes patterned by EBL in an SiO_x oxide [36]).

Due to the existence of a group III droplet at the nanowire tip, this form of growth is group V limited. Krogstrup et al. [37] have argued that diffusion of Ga and As_x on SiO_x, and diffusion of As_x on GaAs nanowire sidewalls, are negligible. Instead, the pathway of group V species (As_x) to the droplet is by desorption from the oxide surface followed by secondary adsorption at the droplet [38, 39]. A similar process may exist for Ga adatoms, in addition to the pathway of diffusion from the nanowire sidewalls.

The self-assisted growth method is primarily motivated by the desire to eliminate any foreign metal catalyst, which may incorporate into and contaminate the nanowires or substrate during growth, leading to deep level defects [40]. Prior studies have shown a reduction in carrier lifetime in Au-catalyzed as compared to Ga-catalyzed GaAs nanowires [41], although recent results contradict this and hence the issue requires further investigation to reach a coherent conclusion [42].

Possibly another benefit of the self-assisted growth method is the lack of parasitic film growth on the oxide surface between the nanowires. This is always a consideration in PV devices, where the thin film that grows simultaneously between the nanowires may contribute to or even dominate the device performance.

Another motivation in the self-assisted growth method is the ability to terminate preferential axial growth by consuming the seed particle with a growth interruption. This technique could be used to facilitate the fabrication of core–shell structures.

The ability to position the group III droplets via holes patterned in the oxide film is beneficial for tuning the spacing between nanowires to maximize light trapping effects (see Section 5). Finally, the self-assisted process is naturally compatible with III–V integration on Si, which could lead to lower cost PV devices (see Section 11).

2.3 SA-MOVPE The selective area MOVPE (SA-MOVPE) method uses patterned holes in an oxide mask to define the location of nanowire growth, similar to the self-assisted growth method but without the need for a metal seed particle [43–45]. In this approach, growth is driven by surface energy anisotropy and preferred growth of certain crystal facets. A review is provided in Ref. [45].

3 Nanowire crystal structure III–V materials (except nitrides) have the zincblende crystal structure in bulk form. Nanowires, on the other hand, typically exhibit polytypism; that is, the crystal structure contains stacking faults (alternating wurtzite and zincblende segments along the nanowire axis), or exhibits zincblende twinning. Hiruma et al. [46–49] reported the first nanometer-scale (10–200 nm in diameter) III–V nanowires grown by Au-assisted VLS and provided valuable information on their crystal structure including transitions from zincblende to wurtzite along the nanowire axis. A review of nanowire crystal structure is provided in Ref. [50]. The wurtzite structure is believed to have a larger bandgap compared to zincblende, and zincblende–wurtzite homostructures are believed to exhibit a type II band alignment [51–53]. The elimination of stacking faults is important since the bandgap fluctuations associated with polytypism are expected to produce carrier scattering (lower carrier mobility), carrier trapping [53, 54] and possible non-radiative recombination.

The prevalence of the wurtzite crystal phase in Au-assisted nanowires was convincingly explained by Glas et al. [55] with subsequent elaborations [56–61], as being caused by preferred nucleation at the VLS triple phase line. In this model, the zincblende phase is favoured at small radii and low supersaturation (for the latter, in the initial stage of growth, or in the final stage of growth upon cool down).

Nearly stacking-fault-free wurtzite GaAs nanowires can be achieved if growth conditions are employed that optimize the droplet chemical potential, surface energies and contact angles such that wurtzite stacking is favoured. Growth conditions that achieve this goal have been reported for MBE-grown GaAs nanowires by employing sufficiently low group III impingement rate and high V/III flux ratio [62]. Similar optimization of growth conditions can reduce or eliminate polytypism in nanowires grown by other techniques such as Au-assisted MOVPE [63, 64] or SA-MOVPE [65, 66].

The zincblende phase is usually favoured in Ga-assisted nanowire growth due to the low Ga surface energy, shape of the Ga droplet, and its wetting of the nanowire sidewalls [61, 67–70]. Recently, the shape of the catalyst has been used to universally explain the polytypism in catalyst-assisted nanowires [37]. The occurrence of other polytypes (e.g., 4H) has been described using *ab initio* [71] and combinatorial models [72].

4 Nanowire growth direction III–V nanowires typically grow in the low energy (111)B direction for zincblende or the (0001) *c*-axis direction for wurtzite as reported early by Hiruma et al. [46–49]. Compound semiconductor (111)B substrates result in III–V nanowires that are orthogonal to the substrate surface [73]. Orthogonal nanowires are preferred to facilitate device processing such as electrical contacting at the tips of the nanowires and to take advantage of optimum light trapping effects (see Section 5). III–V nanowires grown on elemental (111) semiconductor substrates such as (111) Si can result in growth along equivalent ⟨111⟩ directions [73]. III–V nanowires grown on the technologically important Si (100) substrates similarly result in tilted nanowires. However, the preferred growth direction can depend on a wide variety of growth conditions, substrate preparation and pre-nucleation conditions [74–80]. In particular, a 100% yield of vertical nanowires was achieved in Ga-assisted MBE growth of GaAs nanowires on Si (111) substrates by suppression of multiple order twinning at high V/III ratio [81, 82].

Singular growth conditions that lead simultaneously to optimum nanowire morphology (e.g., non-tapered nanowires), stacking fault-free structure and vertical growth direction may not exist (the optimum conditions for morphology may be different than the optimum conditions for crystal structure, for example). In this regard, a change of conditions during growth may be necessary such as the two-temperature method used to optimize the yield of vertical nanowires in the initial stage of growth and nanowire structure later in the growth [83]. In situ HCl etching can also be used to control nanowire morphology independent of growth conditions [84].

5 Optical absorption An important loss mechanism in solar cells is light reflection from the front surface. In conventional cells, this reflection loss can be reduced by employing dielectric anti-reflection coatings or light trapping schemes such as inverted pyramid structures. An array of nanowires can also act as an effective anti-reflection layer with superior wavelength-, polarization-, and angle-dependent properties compared to planar, thin film coatings [85–87].

The anti-reflection properties of nanowires have been well studied both experimentally and theoretically [88–100]. Nanowire dimensions and separation are typically on the order of the wavelength of light where interference effects are dominant; therefore, the reflectance, absorptance and transmittance of nanowire arrays must be determined using wave optics. Li et al. [99] using a full wave finite element method, and Lin et al. [100] using a transfer matrix method, both found that a nanowire diameter near 540 nm and spacing between nanowires (periodicity) near 600 nm optimized the absorptance of the AM 1.5G solar spectrum, thereby imparting a higher PCE in a Si nanowire-based solar cell compared to a Si film of equivalent thickness. The enhanced absorptance was attributed to a field concentration (waveguiding) in the nanowire. Therefore, the optical absorption is greater than that expected from the Lambert–Beer law. Similar enhancements have been reported for Ge [101], GaP [102, 103], InP [103–106] and InAs nanowires [106]. Hu et al. [107, 108] found that a diameter of 180 nm and period (spacing between nanowires) of about 350 nm yielded the highest short-circuit current in a GaAs-on-GaAs or GaAs-on-Si nanowire solar cell. Similar results have been obtained by other groups [105, 106, 109, 110].

Besides tuning the diameter and period of nanowire arrays, absorption and the resulting photocurrent density from a nanowire PV device can also be optimized by increasing the length of nanowires. Figure 2 shows the simulated contribution to the total photocurrent from the nanowires and the substrate in a GaAs nanowire PV device for a nanowire diameter of 180 nm and a period of 350 nm [108]. As the nanowire length increases, the contribution from the nanowire to the total photocurrent increases, while the GaAs substrate contribution correspondingly decreases. The photocurrent from the nanowires saturates for lengths exceeding ~5 μm. The maximum photocurrent of 27.3 mA/cm^2, obtained at 5 μm length, is close to the ideal photocurrent density of 29.9 mA/cm^2 (calculated by integrating the AM1.5G spectrum above the GaAs bandgap). At the optimum nanowire diameter, spacing and length (180 nm, 350 nm, and 5 μm, respectively, for GaAs), we can expect that nanowire growth will be dictated by the

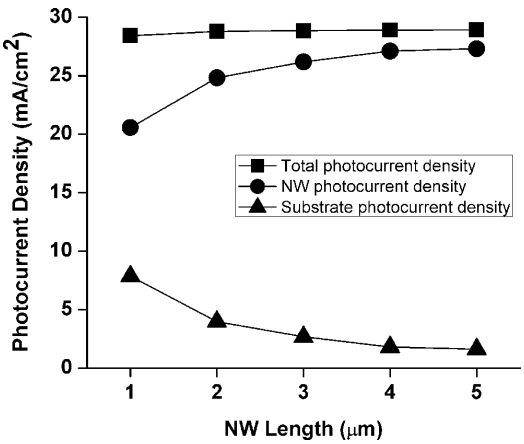

Figure 2 Theoretical contributions from a GaAs nanowire array and the GaAs substrate to the total photocurrent density in a PV device versus nanowire length obtained at a nanowire diameter of 180 nm and period (spacing) of 350 nm. Reprinted with permission from Ref. [108].

shadowing, secondary adsorption and synergetic effects described earlier.

Some interesting work has also been performed on the optical absorption in single nanowires. Resonant absorption has been observed in single nanowires lying horizontally on a substrate [111, 112]. These resonances can be enhanced by engineering the nanowire geometry or adding plasmonic effects with metal nanoparticles [113, 114]. Resonant absorption has also been reported in vertically standing nanowires where a field concentration of 8 was achieved. Consequently, the absorption cross-section of a vertical nanowire is greater than its physical cross-section [115].

6 Carrier collection The advantage of a radial (core–shell) p–n junction nanowire geometry for PV applications was quantitatively assessed in the seminal paper by Kayes et al. [116] and subsequently elaborated by LaPierre [117, 118]. The main advantage of a radial nanowire solar cell is the orthogonal direction of light absorption and carrier collection. Optical absorption is dependent on the nanowire length (as described in Fig. 2), while carrier collection occurs radially along the built-in field of the core–shell p–n junction. Since the nanowire diameter is much less than the carrier diffusion length, internal quantum efficiency (IQE) can approach 100% (i.e., photogenerated carriers are separated and collected at their respective junction before recombination occurs). This means that the efficiency of a GaAs nanowire solar cell can approach the Shockley–Queisser efficiency limit if low surface recombination and certain contacting schemes are employed (see Sections 8 and 9) [117].

7 Strain accommodation and III–V nanowires on Si In planar devices, lattice mismatch strain will result in planar defects (dislocations) if a certain critical thickness is exceeded. The critical thickness in both core–shell [119–125] and axial [126–130] nanowire heterostructures is larger than their thin film counterparts because strain can be relaxed elastically at the nanowire free surface. For a given strain, no dislocations are formed below a certain critical thickness or nanowire radius. This imparts a greater freedom for bandgap engineering in nanowires as compared to thin films. This versatility can be used to optimize PCE in a multi-junction PV cell. Conversely, nanowires which exceed the critical thickness exhibit either dislocations, are kinked, or do not grow at all [126]. A review on dislocations in nanowires is provided in Ref. [131].

One of the primary advantages of the elastic strain relief in nanowires is the ability to integrate III–V nanowires with Si substrates for lower cost PV devices (see Section 11). As discussed earlier, the nanowire diameter required for optimum absorption in an array is 180 nm for GaAs. This diameter can be achieved by significant lateral (radial) overgrowth while maintaining a small contact area to the substrate to avoid dislocations. An example of this is shown in Fig. 3.

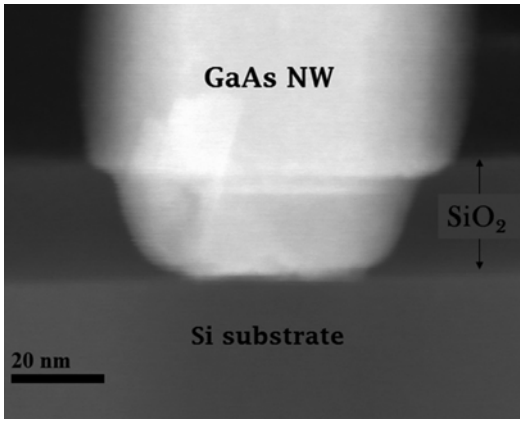

Figure 3 Cross-sectional transmission electron microscopy (TEM) image at the base of a Ga-assisted GaAs nanowire on a patterned SiO_2/Si substrate. The contact area to the substrate is restricted by the oxide hole. Radial growth results in a nanowire that is thicker than its contact area to the Si substrate.

8 Ohmic contact formation Another challenge in nanowire devices may be the realization of low electrical contact resistance. Several papers have discussed the theory of electrical contacts to thin nanowires [132–135]. A review is provided in Ref. [136]. The well-known thermionic field emission theory of contacts seems to apply well to relatively thick nanowires down to diameters of ~140 nm [137]. Metal contacts on the sidewalls of a nanowire can result in carrier depletion due to Fermi level pinning at the nanowire–contact interface. Consequently, the optimum PCE in a PV device is achieved by contacting the top of nanowires instead [117]. A method of planarizing a nanowire array and contacting the top of nanowires was presented in Ref. [138]. Specific contact resistances of III–V/metal contacts, including some III–V/transparent conducting oxide (TCO) contacts [139], are on the order of 10 $\mu\Omega\,cm^2$ for thin films. This is achieved using well-established procedures that include heavy doping under the contact area and thermal annealing [140]. Heurlin et al. [141], for example, used heavy doping to facilitate Ohmic contacting to an InP nanowire. Further information is provided in the section on doping (Section 10). The application of this practice to nanowires can be problematic because the diffusion of the contact material upon annealing can be on the order of 100 nm. Hence, the nanowires must be designed to accommodate this material diffusion and avoid contamination of the p–n junction. Otherwise, diffusion barriers or milder annealing processes may be necessary. Fermi level pinning in the conduction band in InAs can also be employed for Ohmic contact formation [142–144].

9 Passivation Thin nanowires require surface passivation to decrease the density of surface (trap) states on the nanowire sidewalls which lead to detrimental carrier depletion, lower charge carrier mobility, Schottky contacts and carrier recombination. A complete analytical model of

surface depletion was recently presented [145]. An upper limit of 10^{12} cm^{-2} in surface defect density and 10^3 cm/s in surface recombination velocity was calculated to achieve high PCE in a GaAs nanowire PV device [117]. Passivation may be less important in InP, where the surface recombination rate is lower compared to GaAs [146]. Passivation also becomes less important in thick (>150 nm diameter) nanowires [117].

Chemical passivation using chalcogenides, especially sulfur, is one of the most investigated methods for passivation of III–V materials [147], but unfortunately the long term stability of sulfur passivation is inadequate [148, 149]. While sulfur may be used to improve Ohmic contact formation [143], it is doubtful for stable sidewall surface passivation in a real PV device. Instead, the encapsulation of nanowires in a large bandgap passivating shell ("window" layer) is proven to be successful in reducing surface trap density. For example, AlGaAs [150–153] and AlInP [154] are reported as effective passivating shells for GaAs. An InGaP passivating shell was shown to improve the performance of a GaAs PV device [155]. Other results are reported in the section on performance data (Section 15). For electrical contacting, a passivating shell can be locally removed mechanically [154] or by plasma or wet etching technology using published recipes [156].

10 Doping Yet another challenge in nanowire devices is the realization of doping, which is a prerequisite for most optoelectronic devices including PV. High doping is required for the formation of tunnel junctions in multi-junction cells, and for the formation of Ohmic contacts (except for InAs and InN, where a surface accumulation layer occurs due to Fermi level pinning above the conduction band). VLS-mediated growth can result in doping behavior quite different from the thin film case. For example, Si, which is a common n-type dopant for (100) III–V films in MBE, can be p-type on the (111) growth plane of nanowires [157]. Furthermore, the doping incorporation can be different between the VLS-mediated axial growth and the vapour-solid growth on the sidewalls, resulting in inhomogeneous dopant distribution [158, 159] or negligible doping altogether [160]. Diffusion of dopants during growth may also be important [160]. Doping can even affect the nucleation mechanism of nanowires and influence crystal structure [161, 162]. It is commonly assumed that dopant atoms affect the adatom migration on nanowire sidewalls resulting in a tapered morphology [158]. Recently, another model was proposed whereby dopants cause nucleation-limited growth [163]. Finally, doping can affect the composition of ternary III–V alloys [164]. A review on nanowire doping is provided in Ref. [165].

The tools used to evaluate doping in nanowires are becoming increasingly sophisticated. Electrical current-voltage measurements in a four-point probe configuration or in a nanowire-based FET device are the most common method of assessing doping concentration in nanowires. Optical methods for dopant determination include photoluminescence, Raman spectroscopy, and photoconductivity. Scanning probe methods include scanning photocurrent microscopy, Kelvin probe force microscopy and photoemission electron microscopy. Lately, secondary ion mass spectrometry was used on a planarized array of nanowires to assess the depth profile of doping [166], and the Hall effect was recently employed on a single InAs nanowire [167, 168]. Perhaps the most sophisticated tool is atom probe tomography, which provides the three-dimensional distribution of dopant atoms [169]. A discussion of various dopant measurement techniques is provided in Ref. [166].

11 Design for high efficiency PV Most high efficiency planar multi-junction cells use Ge as a substrate, which is a serious drawback due to its expense and scarcity. Several publications have attempted to address this problem by the rational design of alternative nanowire-based PV devices using electrical and optical simulation software [117, 118, 170–172]. For example, the ability to grow nanowires on Si substrates has inspired the design of a two-junction nanowire-on-Si solar cell [118, 173] shown in Fig. 4. The optimum efficiency for a two-junction cell consists of a bottom cell comprised of Si and a top cell with bandgap near 1.7 eV. The limiting efficiency for this cell was calculated to be 33.8% (one Sun illumination) or 42.3% under concentrated light (500 Suns) [118].

In the aforementioned design, a direct bandgap of 1.7 eV for the top nanowire cell can be achieved in a number of compound semiconductor material systems such as $GaAs_{0.77}P_{0.23}$, $Al_{0.19}Ga_{0.81}As$, $In_{0.65}Ga_{0.35}P$, $Al_{0.13}In_{0.87}P$ and $Al_{0.57}In_{0.43}As$ with lattice mismatch to Si of 3.2, 4.1, 5.4, 7.1 and 7.4%, respectively, based on the data by Vurgaftman et al. [174]. Another interesting possibility is $In_xGa_{1-x}N$ alloys which can span the solar spectrum. Of course, other ternary alloys may be of interest for multi-junction cells. The growth of some of these ternary compound semiconductor nanowires, most notably InGaP, AlGaAs and GaAsP, has already been demonstrated on Si or other substrates [175–181]. As discussed previously, the lattice mismatch between the nanowires and Si is not a concern provided the nanowire–substrate contact area is below the critical diameter for dislocations. Among the ternaries listed above, the critical thickness is estimated as 40 nm for the mismatch of 7.4% for $Al_{0.57}In_{0.43}As$ [126]. One of the challenges in the fabrication of ternary alloy semiconductors is achieving a homogeneous composition throughout the nanowire due to the different diffusion lengths or incorporation pathways of the constituent elements in the VLS process [178].

The top contact in Fig. 4 is a transparent conducting oxide (TCO) such as indium tin oxide (ITO) deposited on top of the nanowires. The space between nanowires is filled with a polymer, spin-on glass or other planarizing agent to facilitate a planar top contact of low sheet resistance. Other contacting methods can be employed. For example, an insulating barrier such as SiO_x can be deposited conformally over the nanowires by chemical vapour depo-

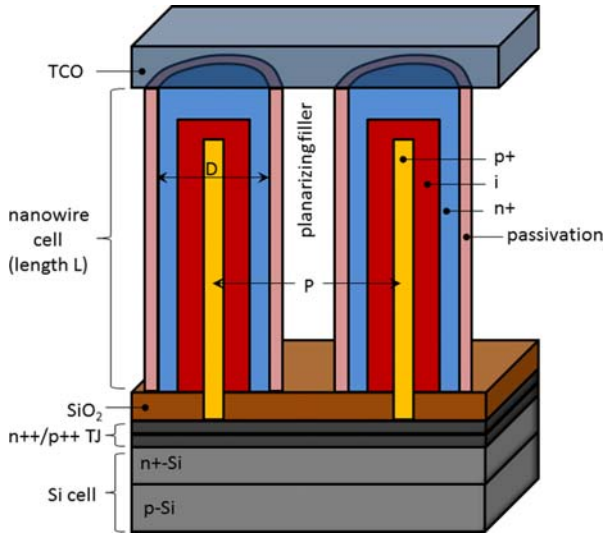

Figure 4 Cross-section through a proposed two-junction nanowire-on-Si solar cell (not to scale). An axial p–i–n structure, rather than the core–shell one presented here, may also be considered. Passivation of the 1.7 eV bandgap nanowires could be accomplished, for example, by a thin shell of InGaP. Nanowire length (L), diameter (D) and period (P) are indicated.

sition. The top of the nanowires are subsequently exposed by a plasma or wet etching process to remove the oxide from the tip of the nanowires. Finally, the TCO can be deposited by atomic layer deposition, sputtering or other methods. The TCO material only makes contact to the top of the nanowires that are exposed through the insulating SiO_x layer.

12 Current-matching The highest efficiency in a series-connected multi-junction cell occurs when the current from each sub-cell is equal, which is the so-called current-matching condition. In thin film solar cells, current-matching is achieved by adjusting the thickness of the absorbing layer in each sub-cell. The diameter (D), length (L) and period (P) in a nanowire array provide additional degrees of freedom to achieve current-matching in a nanowire cell [182]. The parameters (D, L, P) needed for current-matching in a two-junction nanowire-on-Si cell were found to also produce low reflectance and high optical absorption, while the optimum nanowire bandgap was maintained at 1.7 eV [182].

13 Tunnel junctions The design of multi-junction PV requires tunnel junctions (TJ) for a low resistance series connection between sub-cells. Tunnel junctions within nanowires were demonstrated in Refs. [183–185]. Alternatively, a tunnel junction in Si was recently demonstrated [186], suitable for nanowire-on-Si cells.

14 Heterostructures Further improvement in PCE, beyond the nanowire-on-Si cell presented above, may be achieved by tandem p–n heterostructures along the axis of a nanowire that are connected electrically in series by tunnel junctions. As discussed earlier, the freedom from lattice-matching in nanowires permits the optimum bandgaps for higher PCE than can be achieved in thin films. For example, a design for a triple junction nanowire solar cell was presented recently, consisting of two tandem junctions in the nanowire and a third junction in the Si substrate [187].

It is usually assumed from the bulk phase diagrams that group V species (e.g., As, P) have low solubility in Au, while group III species (e.g., In, Ga) have high concentrations in the Au [188]. Hence, group V species are easily depleted from the Au particle during the gas phase switching and abrupt interfaces are easier to achieve in heterostructures where the group III concentration remains constant while the group V species change. This makes InAs/InP and GaAs/GaP nanowires one of the most studied material systems in nanowires. In addition, the InAs/InP and GaAs/GaP nanowire heterostructures are one of the few systems where kinking can be avoided and straight nanowires can be grown due to the kinetics and thermodynamics of growth [189]. Conversely, due to the memory effect of group III species in the droplet, it is more difficult to achieve abrupt heterostructures that involve a change in group III species (e.g. InAs/GaAs, InP/GaAs, GaAs/AlAs, etc.). However, several growth techniques have been developed to achieve abrupt interfaces in the latter situation; for example, one can purge the droplet via a growth interruption [190].

15 Performance data The most relevant metric for the performance of a PV cell is the power conversion efficiency (PCE) given by

$$\eta = \mathrm{FF}\, J_{sc} V_{oc} / I_{inc}\,, \tag{1}$$

where FF is the fill factor, J_{sc} is the short circuit current, V_{oc} is the open circuit voltage, and I_{inc} is the incident irradiance (usually 100 mW/cm^2 for the simulated AM1.5G spectrum). Table 1 summarizes these performance metrics for previously published III–V nanowire-based cells [115, 141, 155, 191–209]. Within each material category, the results are ranked according to the PCE obtained. As can be seen, PCE has risen from ~1% a few years ago to the 10% range today.

Historically, the material of greatest interest in nanowire PV has been either GaAs or InP, because their bandgaps are nearest to the theoretical peak efficiency for a single p–n junction and these materials can be alloyed to produce intermediate bandgaps (e.g., for multi-junction cells). Of course, other ternary alloys are also of interest for multi-junction cells.

With the exception of one report [141], all data in Table 1 is for a single p–n junction. A single nanowire cell with two InP p–n junctions connected in series with a tunnel junction was reported in Ref. [141]. Although not listed in Table 1, it should be mentioned that Lieber's group has done extensive work on Si nanowire solar cells, including

Table 1 Summary of III–V nanowire solar cell performance.

type	substrate	growth details	nanowire (NW) geometry	array or single NW	η *	FF	J_{sc} (mA/cm^2)	V_{oc} (V)	Ref.
GaAs	n-GaAs(111)B	MBE, Au-assisted	core-shell p–n	array	0.83% (2.6 Suns)	26.7% (2.6 Suns)	36.6 (2.6 Suns)	0.2 (2.6 Suns)	[191]
GaAs hybrid	n-GaAs(111)B	MBE, Au-assisted	n-GaAs NWs embedded in P3HT	array	1.04% (2.6 Suns)	N/A	N/A	N/A	[192]
GaAs hybrid	n-GaAs(111)B	SA-MOVPE	n-GaAs NWs embedded in P3HT	array	1.44%	43%	18.6	0.18	[193]
GaAs	p-GaAs(111)B	MBE, Au-assisted	n-type NW on p-type substrate	array	1.65%	25%	27.4	0.245	[194]
GaAs	p-GaAs(111)B	SA-MOVPE	core-shell p–n	array	2.54%	37%	17.6	0.39	[195]
GaAs	Si/SiO_2	solid-source CVD, Au-assisted	Schottky contact	single	2.8%	42%	11	0.6	[196]
GaAs	GaAs(111)B	MBE, self-assisted	core-shell p–i–n	single	4.5%	65%	<0.1	<1	[197]
GaAs	n-GaAs(111)B	SA-MOVPE	core-shell p–n with **InGaP passivation**	array	6.63%	62%	24.3	0.44	[155]
GaAs hybrid	n-GaAs(100)	etched	n-GaAs NWs embedded in PEDOT : PSS	array	9.2%	70%	20.2	0.65	[198]
GaAs	p-Si(111)	MBE, self-catalyzed	core-shell p–i–n	single	40% (due to field concentration)	52%	180 (due to field concentration)	0.43	[115]
InAs	p-Si(111)	MOVPE, catalyst-free	n-type on p-type substrate	array	~1% (300K) 2.5% (110K) (2.86 mW/cm^2)	~55% (2.86 mW/cm^2)	~0.3 (2.86 mW/cm^2)	~0.2 (2.86 mW/cm^2)	[199]
InP hybrid	ITO-coated glass	MOCVD	n-InP NWs embedded in P3HT	array	0.02	44%	2.2×10^{-3}	0.18	[200]
InP	Si(111)	MOVPE, Au-assisted	axial p–i–n with **tandem cell**	single	3.3%	48%	6.0	1.15	[141]
InP	p-InP(111)A	SA-MOVPE	core-shell p–n	array	3.37%	57%	13.7	0.43	[201]
InP	p-InP(111)B	MOVPE, Au-assisted	axial p–i–n	array	13.8%	72.4	24.6	0.779	[202]
InN	n-Si(111)	MBE, catalyst-free	axial p–i–n **CdS passivation**	array	0.68%	34%	14.4	0.14	[203]
GaN	n-Si(111)	CVD, Au-assisted	p-type on n-type Si substrate	array	2.73%	38%	7.6	0.95	[204]
InGaN	sapphire	MOCVD, Ni-catalyst	core-shell n-GaN/ i-$In_xGa_{1-x}N$/ p-GaN	single	0.19%	56%	1.0	0.39	[205]
InGaAs	p-Si(111)	MOVPE, catalyst-free	n-type NWs on p-type Si substrate	array	2.4%	50%	12.9	0.37	[206]
InGaP	GaAs(111)B	MOVPE, Au-assisted	core-shell n-GaAs/InGaP/ p-GaAs	single	4.7%	52%	18.1	0.5	[207]
GaAsP	Si(100)	MOVPE, Au-assisted	core-shell p–n	array	N/A	N/A	0.03 (Ar laser @ 9.6 W/cm^2)	0.11 (Ar laser @ 9.6 W/cm^2)	[208]
GaAsP	p-Si(111)	MBE, self-assisted	core-shell p–i–n **InGaP passivation**	single	10.2%	77%	14.7	0.9	[209]

* Performance parameters were measured at 1 Sun, AM1.5G illumination unless specified otherwise. N/A = not available.

tandem Si PV devices also containing tunnel junctions [210].

Also included in Table 1 are hybrid cells utilizing III–V/polymer junctions [192, 193, 198, 200]. One of these reports [198] describes a cell comprised of nanowires etched from a GaAs substrate. Only a few reports can be found on cells employing III–V ternary alloys for multi-junction PV [205–209].

The record efficiency, reported recently, is $\eta = 13.8\%$ for a Au-assisted InP axial p–i–n nanowire array on an InP (111)B substrate [202]. The success of this device is possibly attributed to its patterned array, more optimal geometry (diameter, pitch, length), and the use of InP with its lower surface recombination velocity.

Table 1 also includes results from single nanowire solar cells. All of the single nanowire results, except for Ref. [115], are obtained from nanowires transferred horizontally to a host substrate. Single nanowire results typically have higher efficiency compared to nanowire arrays due to difficulty in processing larger areas and avoiding short circuit paths. An important result for horizontally lying nanowires is a 10.2% efficient GaAsP single nanowire solar cell with InGaP passivation grown on Si [209]. Only one report [115] is for a single nanowire solar cell from a single as-grown nanowire still oriented vertically on a Si substrate. Caution is warranted in the interpretation of single nanowire results, particularly Ref. [115], due to field concentration effects and problems in defining the area and hence the PCE. As described in the section on optical absorption, it is clear that nanowires absorb light from their surroundings. This makes comparison with arrays difficult.

The results in Table 1 should be compared to the record efficiencies for thin film cells. The record one Sun efficiencies are 28.8% for GaAs, 22.1% for InP, and 37.5% for a triple-junction thin film cell [6]. Further work is clearly required for nanowires to have comparable efficiency.

16 Other opportunities

16.1 Further cost reduction To further reduce cost, there is interest in growing nanowires on other substrates such as ITO, glass, metal foil, graphite or even graphene [211–215]. Some of these, such as metal foil and graphene, would enable flexible devices with applications in building integrated PV and consumer electronics. Such devices also have potentially lower costs of installation. However, nanowires grown on these substrates are usually randomly oriented which is non-optimal for contacting and light trapping. Flexible PV devices could also be fabricated by the transfer of nanowires into a polymer film with the potential to recycle the substrate [216–218]. Finally, a new process, called "aerotaxy", involving bulk fabrication of III–V nanowires, was recently published [219], which might satisfy the need for low cost III–V nanowire production.

16.2 Other third generation concepts Other third generation concepts to improve PCE include multiple exciton generation (MEG) and hot carrier solar cells [3]. MEG increases the photocurrent of a cell by using the energy lost by carrier relaxation to produce additional electron–hole pairs. This effect is being investigated primarily in II–VI quantum dots. On the other hand, hot carrier solar cells increase the photovoltage of a cell by extracting the carriers before thermalization can occur. In hot carrier cells, a resonant tunneling contact structure is required to extract the hot carriers. The ability to incorporate quantum dot heterostuctures, superlattices, and resonant tunneling structures into nanowires could facilitate novel designs for MEG or hot carrier cells.

17 Conclusion and grand challenges

In summary, the following attributes are required for high PCE:

1. controlled nanowire morphology;
2. stacking-fault-free crystalline structure;
3. orthogonal nanowires with optimum diameter (D), period (P) and length (L) to maximize optical absorption;
4. patterned arrays using cost effective processes (perhaps nanoimprint lithography);
5. dimensions below the critical thickness or critical diameter to avoid misfit dislocations;
6. removal of catalyst droplet to avoid reflection loss and/or Schottky barrier contacts at the tip of nanowires, and possible elimination of Au as a catalyst due to deep level defects;
7. low resistance contacts necessitating highly doped contact layers;
8. controlled doping for p–i–n junctions;
9. surface passivation;
10. current-matching with high performance tunnel junctions; and
11. proven reliability.

As highlighted in this article, some of these items are highly developed (such as item 4, patterned arrays), while others require extensive investigation. Regarding the last point, many of the materials and processes proposed for nanowire PV are already used in existing thin film PV (flat panels for space applications and terrestrial concentrator PV systems) and telecommunications systems (laser diodes, photodetectors) that already meet stringent reliability standards. Nevertheless, nanowire-based devices will eventually have to undergo rigorous qualification testing as described by various organizations (such as the International Electrotechnical Commission (IEC) 61215 test standard) as a prerequisite for any commercially viable PV technology.

Considerable progress toward nanowire PV has already been made as outlined in the previous sections. Nanowire solar cells could provide a low cost, high efficiency option for the concentrator PV market. Besides leading to more cost effective large-scale solar farms, a low cost concentrator PV cell would also lead to more widespread implementation of these systems – for example, in areas of relatively low insolation or in commercial roof-top applications, which would provide much higher power than conven-

tional silicon-based flat modules and make much better use of land or roof-top area.

Acknowledgements The authors wish to thank the financial support of the Natural Sciences and Engineering Research Council of Canada.

References

[1] World Energy Council, World Energy Issues Monitor 2013.
[2] Intergovernmental Panel on Climate Change, Climate Change 2007: Mitigation of Climate Change.
[3] M. A. Green, Third generation photovoltaics: Ultra-high conversion efficiency at low cost, Prog. Photovolt.: Res. Appl. **9**, 123 (2001).
[4] W. Shockley and H. J. Queisser, Detailed balance limit of efficiency of p–n junction solar cells, J. Appl. Phys. **32**, 510 (1961).
[5] F. Dimroth and S. Kurtz, High-efficiency multijunction solar cells, MRS Bull. **32**, 230 (2007).
[6] M. A. Green, K. Emery, Y. Hishikawa, W. Warta, and E. D. Dunlop, Solar cell efficiency tables (version 41), Prog. Photovolt. Res. Appl. **21**, 1 (2013).
[7] A. Luque and V. Andreev (eds.), Concentrator Photovoltaics (Springer, Berlin, 2007).
[8] S. Chattopadhyay, L.-C. Chen and K.-H. Chen, Energy production and conversion applications of one-dimensional semiconductor nanostructures, NPG Asia Mater. **3**, 74 (2011).
[9] K. Sun, A. Kargar, N. Park, K. N. Madsen, P. W. Naughton, T. Bright, Y. Jing, and D. Wang, Compound semiconductor nanowire solar cells, IEEE J. Sel. Top. Quantum Electron. **17**, 1033 (2011).
[10] Z. Fan, D. J. Ruebusch, A. A. Rathore, R. Kapadia, O. Ergen, P. W. Leu, and Ali Javey, Challenges and prospects of nanopillar-based solar cells, Nano Res. **2**, 829 (2009).
[11] M. T. Borgstrom, J. Wallentin, M. Heurlin, S. Falt, P. Wickert, J. Leene, M. H. Magnusson, K. Deppert, and L. Samuelson, Nanowires with promise for photovoltaics, IEEE J. Sel. Top. Quantum Electron. **17**, 1050 (2011).
[12] L. Tsakalakos, Nanostructures for photovoltaics, Mater. Sci. Eng. R. **62**, 175 (2008).
[13] A. M. Morales and C. M. Lieber, A laser ablation method for the synthesis of crystalline semiconductor nanowires, Science **279**, 208 (1998).
[14] R. S. Wagner and W. C. Ellis, Vapor–liquid–solid mechanism of single crystal growth, Appl. Phys. Lett. **4**, 89 (1964).
[15] E. I. Givargizov, Fundamental aspects of VLS growth, J. Cryst. Growth **31**, 20 (1975).
[16] M. E. Messing, K. Hillerich, J. Bolinsson, K. Storm, J. Johansson, K. A. Dick, and K. Deppert, A comparative study of the effect of gold seed particle preparation method on nanowire growth, Nano Res. **3**, 506 (2010).
[17] A. Gustafsson, K. Hillerich, M. E. Messing, K. Storm, K. A. Dick, K. Deppert, and J. Bolinsson, A cathodoluminescence study of the influence of the seed particle preparation method on the optical properties of GaAs nanowires, Nanotechnology **23**, 265704 (2012).
[18] T. Martensson, M. Borgstrom, W. Seifert, B. J. Ohlsson, and L. Samuelson, Fabrication of individually seeded nanowire arrays by vapour–liquid–solid growth, Nanotechnology **14**, 1255 (2003).
[19] T. Martensson, P. Carlberg, M. Borgstrom, L. Montelius, W. Seifert, and L. Samuelson, Nanowire arrays defined by nanoimprint lithography, Nano Lett. **4**, 699 (2004).
[20] V. G. Dubrovskii, M. A. Timofeeva, and M. Tchernycheva, Lateral growth and shape of semiconductor nanowires, Semiconductors **47**, 50 (2013).
[21] V. G. Dubrovskii, N. V. Sibirev, G. E. Cirlin, I. P. Soshnikov, W. H. Chen, R. Larde, E. Cadel, P. Pareige, T. Xu, B. Grandidier, J.-P. Nys, D. Stievenard, M. Moewe, L. C. Chuang, and C. Chang-Hasnain, Gibbs-Thomson and diffusion-induced contributions to the growth rate of Si, InP, and GaAs nanowires, Phys. Rev. B **79**, 205316 (2009).
[22] N. V. Sibirev, V. G. Dubrovskii, G. E. Cirlin, V. A. Egorov, Y. B. Samsonenko, and V. M. Ustinov, Deposition-rate dependence of the height of GaAs-nanowires, Semiconductors **42**, 1259 (2008).
[23] V. G. Dubrovskii, N. V. Sibirev, G. E. Cirlin, M. Tchernycheva, J. C. Harmand, and V. M. Ustinov, Shape modification of III–V nanowires: The role of nucleation on sidewalls, Phys. Rev. E **77**, 031606 (2008).
[24] V. G. Dubrovskii, N. V. Sibirev, R. A. Suris, G. E. Cirlin, J. C. Harmand, and V. M. Ustinov, Diffusion-controlled growth of semiconductor nanowires: Vapor pressure versus high vacuum deposition, Surf. Sci. **601**, 4395 (2007).
[25] J.-C. Harmand, F. Glas, and G. Patriarche, Growth kinetics of a single $InP_{1-x}As_x$ nanowire, Phys. Rev. B **81**, 235436 (2010).
[26] O. Salehzadeh and S. P. Watkins, Control of GaAs nanowire morphology by group III precursor chemistry, J. Cryst. Growth **325**, 5 (2011).
[27] H. Xu, Y. Wang, Y. Guo, Z. Liao, Q. Gao, N. Jiang, H. H. Tan, C. Jagadish, and J. Zou, High-density, defect-free, and taper-restrained epitaxial GaAs nanowires induced from annealed Au thin films, Cryst. Growth Des. **12**, 2018 (2012).
[28] N. V. Sibirev, M. Tchernycheva, M. A. Timofeeva, J. C. Harmand, G. E. Cirlin, and V. G. Dubrovskii, Influence of shadow effect on the growth and shape of InAs nanowires, J. Appl. Phys. **111**, 104317 (2012).
[29] M. T. Borgstrom, G. Immink, B. Ketelaars, R. Algra, and E. P. A. M. Bakkers, Synergetic nanowire growth, Nature Nanotechnol. **2**, 541 (2007).
[30] S. Plissard, K. A. Dick, G. Larrieu, S. Godey, A. Addad, X. Wallart, and P. Caroff, Gold-free growth of GaAs nanowires on silicon: arrays and polytypism, Nanotechnology **21**, 385602 (2010).
[31] B. Bauer, A. Rudolph, M. Soda, A. Fontcuberta i Morral, J. Zweck, D. Schuh, and E. Reiger, Position controlled self-catalyzed growth of GaAs nanowires by molecular beam epitaxy, Nanotechnology **21**, 435601 (2010).
[32] A. Fontcuberta i Morral, C. Colombo, G. Abstreiter, J. Arbiol, and J. R. Morante, Nucleation mechanism of gallium-assisted molecular beam epitaxy growth of gallium arsenide nanowires, Appl. Phys. Lett. **92**, 063112 (2008).
[33] B. Mandl, J. Stangl, E. Hilner, A. A. Zakharov, K. Hillerich, A. W. Dey, L. Samuelson, G. Bauer, K. Deppert, and A. Mikkelsen, Growth mechanism of self-catalyzed group III–V nanowires, Nano Lett. **10**, 4443 (2010).
[34] A. Fontcuberta i Morral, Gold-Free GaAs Nanowire Synthesis and Optical Properties, IEEE J. Sel. Top. Quantum Electron. **17**, 819 (2011).

[35] C. Colombo, D. Spirkoska, M. Frimmer, G. Abstreiter, and A. Fontcuberta i Morral, Ga-assisted catalyst-free growth mechanism of GaAs nanowires by molecular beam epitaxy, Phys. Rev. B **77**, 155326 (2008).
[36] S. Plissard, G. Larrieu, X. Wallart, and P. Caroff, High yield of self-catalyzed GaAs nanowire arrays grown on silicon via gallium droplet positioning, Nanotechnology **22**, 275602 (2011).
[37] P. Krogstrup, H. I. Jørgensen, E. Johnson, M. H. Madsen, C. B. Sørensen, A. Fontcuberta i Morral, M. Aagesen, J. Nygård, and F. Glas, Theoretical formalism and modeling of III–V nanowire growth dynamics, arXiv:1301.7441 [cond-mat.mes-hall].
[38] M. R. Ramdani, J. C. Harmand, F. Glas, G. Patriarche, and L. Travers, Arsenic Pathways in Self-Catalyzed Growth of GaAs Nanowires, Cryst. Growth Des. **13**, 91 (2013).
[39] D. Dalacu, A. Kam, D. G. Austing, X. Wu, J. Lapointe, G. C Aers, and P. J. Poole, Selective-area vapour–liquid–solid growth of InP nanowires, Nanotechnology **20**, 395602 (2009).
[40] M. Bar-Sadan, J. Barthel, H. Shtrikman, and L. Houben, Direct imaging of single Au atoms within GaAs nanowires, Nano Lett. **12**, 2352 (2012).
[41] S. Breuer, C. Pfuller, T. Flissikowski, O. Brandt, H. T. Grahn, L. Geelhaar, and H. Riechert, Suitability of Au- and self-assisted GaAs nanowires for optoelectronic applications, Nano Lett. **11**, 1276 (2011).
[42] L. Ahtapodov, J. Todorovic, P. Olk, T. Mjåland, P. Slåttnes, D. L. Dheeraj, A. T. J. van Helvoort, B.-O. Fimland, and H. Weman, A story told by a single nanowire: optical properties of wurtzite GaAs, Nano Lett. **12**, 6090 (2012).
[43] K. Ikejiri, J. Noborisaka, S. Hara, J. Motohisa, and T. Fukui, Mechanism of catalyst-free growth of GaAs nanowires by selective area MOVPE, J. Cryst. Growth **298**, 616 (2007).
[44] D. Rudolph, S. Hertenberger, S. Bolte, W. Paosangthong, D. Spirkoska, M. Doblinger, M. Bichler, J. J. Finley, G. Abstreiter, and G. Koblmuller, Direct observation of a noncatalytic growth regime for GaAs nanowires, Nano Lett. **11**, 3848 (2011).
[45] K. Tomiokaa, K. Ikejiri, T. Tanaka, J. Motohisa, S. Hara, K. Hiruma, and T. Fukui, Selective-area growth of III–V nanowires and their applications, J. Mater. Res. **26**, 2127 (2011).
[46] K. Hiruma, T. Katsuyama, K. Ogawa, M. Koguchi, H. Kakibayashi, and G. P. Morgan, Quantum size microcrystals grown using organometallic vapor phase epitaxy, Appl. Phys. Lett. **59**, 431 (1991).
[47] M. Yazawa, M. Koguchi, A. Muto, M. Ozawa, and K. Hiruma, Effect of one monolayer of surface gold atoms on the epitaxial growth of InAs nanowhiskers, Appl. Phys. Lett. **61**, 2051 (1992).
[48] M. Koguchi, H. Kakibayashi, M. Yazawa, K. Hiruma, and T. Katsuyama, Crystal structure change of GaAs and InAs whiskers from zinc-blende to wurtzite type, Jpn. J. Appl. Phys. **31**, 2061 (1992).
[49] K. Hiruma, M. Yazawa, K. Haraguchi, K. Ogawa, T. Katsuyama, M. Koguchi, and H. Kakibayashi, GaAs free-standing quantum-size wires, J. Appl. Phys. **74**, 3162 (1993).
[50] K. A. Dick, P. Caroff, J. Bolinsson, M. E. Messing, J. Johansson, K. Deppert, L. R. Wallenberg, and L. Samuelson, Control of III–V nanowire crystal structure by growth parameter tuning, Semicond. Sci. Technol. **25**, 024009 (2010).
[51] M. Heiss, S. Conesa-Boj, J. Ren, H.-H. Tseng, A. Gali, A. Rudolph, E. Uccelli, F. Peir, J. R. Morante, D. Schuh, E. Reiger, E. Kaxiras, J. Arbiol, and A. Fontcuberta i Morral, Direct correlation of crystal structure and optical properties in wurtzite/zinc-blende GaAs nanowire heterostructures, Phys. Rev. B **83**, 045303 (2011).
[52] J. Bao, D. C. Bell, and F. Capasso, Optical properties of rotationally twinned InP nanowire heterostructures, Nano Lett. **8**, 836 (2008).
[53] K. Pemasiri, M. Montazeri, R. Gass, L. M. Smith, H. E. Jackson, J. Yarrison-Rice, S. Paiman, Q. Gao, H. H. Tan, C. Jagadish, X. Zhang, and J. Zou, Carrier dynamics and quantum confinement in type II ZB–WZ InP nanowire homostructures, Nano Lett. **9**, 648 (2009).
[54] J. Wallentin, M. Ek, L. R. Wallenberg, L. Samuelson, and M. T. Borgström, Electron trapping in InP nanowire FETs with stacking faults, Nano Lett. **12**, 151 (2012).
[55] F. Glas, J. C. Harmand, and G. Patriarche, Why does wurtzite form in nanowires of III–V zinc blende semiconductors?, Phys. Rev. Lett. **9**, 146101 (2007).
[56] V. G. Dubrovskii and N. V. Sibirev, Growth thermodynamics of nanowires and its application to polytypism of zinc blende III–V nanowires, Phys. Rev. B **77**, 035414 (2008).
[57] V. G. Dubrovskii, N. V. Sibirev, J. C. Harmand, and F. Glas, Growth kinetics and crystal structure of semiconductor nanowires, Phys. Rev. B **78**, 235301 (2008).
[58] N. V. Sibirev, M. A. Timofeeva, A. D. Bolshakov, M. V. Nazarenko, and V. G. Dubrovskii, Surface energy and crystal structure of nanowhiskers of III–V semiconductor compounds, Phys. Solid State **52**, 1531 (2010).
[59] M. V. Nazarenko, N. V. Sibirev, and V. G. Dubrovskii, Self-Consistent Model of nanowire growth and crystal structure with regard to the adatom diffusion source, Tech. Phys. **56**, 311 (2011).
[60] X. Ren, H. Huang, V. G. Dubrovskii, N. V. Sibirev, M. V. Nazarenko, A. D. Bolshakov, X. Ye, Q. Wang, Y. Huang, X. Zhang, J. Guo, and X. Liu, Experimental and theoretical investigations on the phase purity of GaAs zincblende nanowires, Semicond. Sci. Technol. **26**, 014034 (2011).
[61] R. E. Algra, M. A. Verheijen, L.-F. Feiner, G. G. W. Immink, W. J. P. van Enckevort, E. Vlieg, and E. P. A. M. Bakkers, The role of surface energies and chemical potential during nanowire growth, Nano Lett. **11**, 1259 (2011).
[62] M. C. Plante and R. R. LaPierre, Control of GaAs nanowire morphology and crystal structure, Nanotechnology **19**, 495603 (2008).
[63] J. H. Kang, Q. Gao, P. Parkinson, H. J. Joyce, H. H. Tan, Y. Kim, Y. Guo, H. Xu, J. Zou, and C. Jagadish, Precursor flow rate manipulation for the controlled fabrication of twin-free GaAs nanowires on silicon substrates, Nanotechnology **23**, 415702 (2012).
[64] H. J. Joyce, J. Wong-Leung, Q. Gao, H. H. Tan, and C. Jagadish, Phase perfection in zinc blende and wurtzite III–V nanowires using basic growth parameters, Nano Lett. **10**, 908 (2010).
[65] Y. Kitauchi, Y. Kobayashi, K. Tomioka, S. Hara, K. Hiruma, T. Fukui, and J. Motohisa, Structural transition in indium phosphide nanowires, Nano Lett. **10**, 1699 (2010).

[66] H. Yoshida, K. Ikejiri, T. Sato, S. Hara, K. Hiruma, J. Motohisa, and T. Fukui, Analysis of twin defects in GaAs nanowires and tetrahedral and their correlation to GaAs (111)B surface reconstructions in selective-area metalorganic vapour-phase epitaxy, J. Cryst. Growth **312**, 52 (2009).
[67] V. G. Dubrovskii, G. E. Cirlin, N. V. Sibirev, F. Jabeen, J. C. Harmand, and P. Werner, New mode of vapor–liquid–solid nanowire growth, Nano Lett. **11**, 1247 (2011).
[68] P. Krogstrup, S. Curiotto, E. Johnson, M. Aagesen, J. Nygard, and D. Chatain, Impact of the liquid phase shape on the structure of III–V nanowires, Phys. Rev. Lett. **106**, 125505 (2011).
[69] P. Krogstrup, R. Popovitz-Biro, E. Johnson, M. H. Madsen, J. Nygård, and H. Shtrikman, Structural phase control in self-catalyzed growth of GaAs nanowires on silicon (111), Nano Lett. **10**, 4475 (2010).
[70] G. E. Cirlin, V. G. Dubrovskii, Y. B. Samsonenko, A. D. Bouravleuv, K. Durose, Y. Y. Proskuryakov, B. Mendes, L. Bowen, M. A. Kaliteevski, R. A. Abram, and D. Zeze, Self-catalyzed, pure zincblende GaAs nanowires grown on Si(111) by molecular beam epitaxy, Phys. Rev. B **82**, 035302 (2010).
[71] C. Panse, D. Kriegner, and F. Bechstedt, Polytypism of GaAs, InP, InAs, and InSb: An ab initio study, Phys. Rev. B **84**, 075217 (2011).
[72] J. Johansson, J. Bolinsson, M. Ek, P. Caroff, and K. A. Dick, Combinatorial approaches to understanding polytypism in III–V nanowires, ACS Nano **6**, 6142 (2012).
[73] S. A. Fortuna and X. Li, Metal-catalyzed semiconductor nanowires: a review on the control of growth directions, Semicond. Sci. Technol. **25**, 024005 (2010).
[74] K. Ikejiri, F. Ishizaka, K. Tomioka, and T. Fukui, Bidirectional growth of indium phosphide nanowires, Nano Lett. **12**, 4770 (2012).
[75] S. T. Boles, C. V. Thompson, and E. A. Fitzgerald, Influence of indium and phosphine on Au-catalyzed InP nanowire growth on Si substrates, J. Cryst. Growth **311**, 1446 (2009).
[76] X.-Y. Bao, C. Soci, D. Susac, J. Bratvold, D. P. R. Aplin, W. Wei, C.-Y. Chen, S. A. Dayeh, K. L. Kavanagh, and D. Wang, Heteroepitaxial growth of vertical GaAs nanowires on Si(111) substrates by metal-organic chemical vapor deposition, Nano Lett. **8**, 3755 (2008).
[77] M. Mattila, T. Hakkarainen, H. Jiang, E. I. Kauppinen, and H. Lipsanen, Effect of substrate orientation on the catalyst-free growth of InP nanowires, Nanotechnology **18**, 155301 (2007).
[78] K. Tomioka, J. Motohisa, S. Hara, and T. Fukui, Control of InAs nanowire growth directions on Si, Nano Lett. **8**, 3475 (2008).
[79] J. H. Kang, Q. Gao, H. J. Joyce, H. H. Tan, C. Jagadish, Y. Kim, D. Y. Choi, Y. Guo, H. Xu, J. Zou, M. A. Fickenscher, L. M. Smith, H. E. Jackson, and J. M. Yarrison-Rice, Novel growth and properties of GaAs nanowires on Si substrates, Nanotechnology **21**, 035604 (2010).
[80] U. Krishnamachari, M. Borgstrom, B. J. Ohlsson, N. Panev, L. Samuelson, W. Seifert, M. W. Larsson, and L. R. Wallenberg, Defect-free InP nanowires grown in [001] direction on InP(001), Appl. Phys. Lett. **85**, 2077 (2004).
[81] E. Uccelli, J. Arbiol, C. Magen, P. Krogstrup, E. Russo-Averchi, M. Heiss, G. Mugny, F. Morier-Genoud, J. Nygard, J. R. Morante, and A. Fontcuberta i Morral, Three-dimensional multiple-order twinning of self-catalyzed GaAs nanowires on Si substrates, Nano Lett. **11**, 3827 (2011).
[82] E. Russo-Averchi, M. Heiss, L. Michelet, P. Krogstrup, J. Nygard, C. Magen, J. R. Morante, E. Uccelli, J. Arbiol, and A. Fontcuberta i Morral, Suppression of three dimensional twinning for a 100% yield of vertical GaAs nanowires on silicon, Nanoscale **4**, 1486 (2012).
[83] H. J. Joyce, Q. Gao, H. H. Tan, C. Jagadish, Y. Kim, X. Zhang, Y. Guo, and J. Zou, Twin-free uniform epitaxial GaAs nanowires grown by a two-temperature process, Nano Lett. **7**, 921 (2007).
[84] M. T. Borgstrom, J. Wallentin, J. Tragardh, P. Ramvall, M. Ek, L. R. Wallenberg, L. Samuelson, and K. Deppert, In situ etching for total control over axial and radial nanowire growth, Nano Res. **3**, 264 (2010).
[85] S. L. Diedenhofen, G. Grzela, E. Haverkamp, G. Bauhuis, J. Schermer, and J. G. Rivas, Broadband and omnidirectional anti-reflection layer for III/V multi-junction solar cells, Sol. Energy Mater. Sol. Cells **101**, 308 (2012).
[86] S. L. Diedenhofen, G. Vecchi, R. E. Algra, A. Hartsuiker, O. L. Muskens, G. Immink, E. P. A. M. Bakkers, W. L. Vos, and J. G. Rivas, Broad-band and Omnidirectional Antireflection Coatings Based on Semiconductor Nanorods, Adv. Mater. **21**, 973 (2009).
[87] J. Zhu, Z. Yu, S. Fan, and Y. Cui, Nanostructured photon management for high performance solar cells, Mater. Sci. Eng. R **70**, 330 (2010).
[88] S. Jeong, S. Wang, and Yi Cui, Nanoscale photon management in silicon solar cells, J. Vac. Sci. Technol. A **30**, 060801 (2012).
[89] L. Tsakalakos, J. Balch, J. Fronheiser, M. Y. Shih, S. F. LeBoeuf, M. Pietrzykowski, P. J. Codella, B. A. Korevaar, O. Sulima, J. Rand, A. Davuluru, and U. Rapol, Strong broadband optical absorption in silicon nanowire films, J. Nanophoton. **1**, 013552 (2007).
[90] W. Q. Xie, J. I. Oh, and W. Z. Shen, Realization of effective light trapping and omnidirectional antireflection in smooth surface silicon nanowire arrays, Nanotechnology **22**, 065704 (2011).
[91] A. Convertino, M. Cuscuna, and F. Martelli, Optical reflectivity from highly disordered Si nanowire films, Nanotechnology **21**, 355701 (2010).
[92] J. Zhu, Z. Yu, G. F. Burkhard, C.-M. Hsu, S. T. Connor, Y. Xu, Q. Wang, M. McGehee, S. Fan, and Y. Cui, Optical absorption enhancement in amorphous silicon nanowire and nanocone arrays, Nano Lett. **9**, 279 (2009).
[93] S. K. Srivastava, D. Kumar, P. K. Singh, M. Kar, V. Kumar, and M. Husain, Excellent antireflection properties of vertical silicon nanowire arrays, Sol. Energy Mater. Sol. Cells **94**, 1506 (2010).
[94] X. Li, J. Li, T. Chen, B. K. Tay, J. Wang, and H. Yu, Periodically aligned Si nanopillar arrays as efficient antireflection layers for solar cell applications, Nanoscale Res. Lett. **5**, 1721 (2010).
[95] E. Garnett and P. Yang, Light trapping in silicon nanowire solar cells, Nano Lett. **10**, 1082 (2010).
[96] Z. Xiong, F. Zhao, J. Yang, and X. Hu, Comparison of optical absorption in Si nanowire and nanoporous Si structures

for photovoltaic applications, Appl. Phys. Lett. **96**, 181903 (2010).
[97] L. Hu and G. Chen, Analysis of optical absorption in silicon nanowire arrays for photovoltaic applications, Nano Lett. **7**, 3249 (2007).
[98] J. Li, H. Yu, S. M. Wong, G. Zhang, X. Sun, P. G.-Q. Lo, and D.-L. Kwong, Si nanopillar array optimization on Si thin films for solar energy harvesting, Appl. Phys. Lett. **95**, 033102 (2009).
[99] J. Li, H. Yu, S. M. Wong, X. Li, G. Zhang, P. G.-Q. Lo, and D.-L. Kwong, Design guidelines of periodic Si nanowire arrays for solar cell application, Appl. Phys. Lett. **95**, 243113 (2009).
[100] C. Lin and M. L. Povinelli, Optical absorption enhancement in silicon nanowire arrays with a large lattice constant for photovoltaic applications, Opt. Express **17**, 19371 (2009).
[101] Z. Y. Fan, R. Kapadia, P. W. Leu, X. B. Zhang, Y. L. Chueh, K. Takei, K. Yu, A. Jamshidi, A. A. Rathore, D. J. Ruebusch, M. Wu, and A. Javey, Ordered arrays of dual-diameter nanopillars for maximized optical absorption, Nano Lett. **10**, 3823 (2010).
[102] S. L. Diedenhofen, G. Vecchi, R. E. Algra, A. Hartsuiker, O. L. Muskens, G. Immink, E. P. A. M. Bakkers, W. L. Vos, and J. G. Rivas, Broad-band and omnidirectional antireflection coatings based on semiconductor nanorods, Adv. Mater. **21**, 973 (2009).
[103] O. L. Muskens, J. G. Rivas, R. E. Algra, E. P. A. M. Bakkers, and A. Lagendijk, Design of light scattering in nanowire materials for photovoltaic applications, Nano Lett. **8**, 2638 (2008).
[104] N. Anttu and H. Q. Xu, Coupling of light into nanowire arrays and subsequent absorption, J. Nanosci. Nanotechnol. **10**, 7183 (2010).
[105] J. Kupec, R. L. Stoop, and B. Witzigmann, Light absorption and emission in nanowire array solar cells, Opt. Express **18**, 27589 (2010).
[106] J. Kupec and B. Witzigmann, Dispersion, wave propagation and efficiency analysis of nanowire solar cells, Opt. Express **17**, 10399 (2009).
[107] Y. Hu, M. Li, J.-J. He, and R. R. LaPierre, Current matching and efficiency optimization in a two-junction nanowire-on-silicon solar cell, Nanotechnology **24**, 065402 (2013).
[108] Y. Hu, R. R. LaPierre, M. Li, K. Chen, and J.-J. He, Optical characteristics of GaAs nanowire solar cells, J. Appl. Phys. **112**, 104311 (2012).
[109] L. Wen, Z. Zhao, X. Li, Y. Shen, H. Guo, and Y. Wang, Theoretical analysis and modeling of light trapping in high efficicency GaAs nanowire array solar cell, Appl. Phys. Lett. **99**, 143116 (2011).
[110] J. Motohisa and K. Hiruma, Light absorption in semiconductor nanowire arrays with multijunction cell structures, Jpn. J. Appl. Phys. **51**, 11PE07 (2012).
[111] M. Heiss and A. Fontcuberta i Morral, Fundamental limits in the external quantum efficiency of single nanowire, Appl. Phys. Lett. **99**, 263102 (2011).
[112] L. Cao, J. S. White, J.-S. Park, J. A. Schuller, B. M. Clemens, and M. L. Brongersma, Engineering light absorption in semiconductor nanowire devices, Nature Mater. **8**, 643 (2009).
[113] X. Li and Y. Zhan, Enhanced external quantum efficiency in rectangular single nanowire solar cells, Appl. Phys. Lett. **102**, 021101 (2013).
[114] C. Colombo, P. Krogstrup, J. Nygård, M. L. Brongersma, and A. Fontcuberta i Morral, Engineering light absorption in single-nanowire solar cells with metal nanoparticles, New J. Phys. **13**, 123026 (2011).
[115] P. Krogstrup, H. I. Jørgensen, M. Heiss, O. Demichel, J. V. Holm, M. Aagesen, J. Nygard, and A. Fontcuberta i Morral, Single nanowire solar cells beyond the Shockley-Queisser limit, Nature Photon. **7**, 306 (2013).
[116] B. M. Kayes, H. A. Atwater, and N. S. Lewis, Comparison of the device physics principles of planar and radial p–n junction nanorod solar cells, J. Appl. Phys. **97**, 114302 (2005).
[117] R. R. LaPierre, Numerical model of current-voltage characteristics and efficiency of GaAs nanowire solar cells, J. Appl. Phys. **109**, 034311 (2011).
[118] R. R. LaPierre, Theoretical conversion efficiency of a two-junction nanowire on Si solar cell, J. Appl. Phys. **110**, 014310 (2011).
[119] T. E. Trammell, X. Zhang, Y. Li, L.-Q. Chen, and E. C. Dickey, Equilibrium strain-energy analysis of coherently strained core–shell nanowires, J. Cryst. Growth **310**, 3084 (2008).
[120] S. Raychaudhuri and E. T. Yu, Critical dimensions in coherently strained coaxial nanowire heterostructures, J. Appl. Phys. **99**, 114308 (2006).
[121] K. L. Kavanagh, I. Saveliev, M. Blumin, G. Swadener, and H. E. Ruda, Faster radial strain relaxation in InAs–GaAs core–shell heterowires, J. Appl. Phys. **111**, 044301 (2012).
[122] S. Raychaudhuri and E. T. Yu, Calculation of critical dimensions for wurtzite and cubic zinc blende coaxial nanowire heterostructures, J. Vac. Sci. Technol. B **24**, 2053 (2006).
[123] M. Y. Gutkin, K. V. Kuzmin, and A. G. Sheinerman, Misfit stresses and relaxation mechanisms in a nanowire containing a coaxial cylindrical inclusion of finite height, Phys. Status Solidi B **248**, 1651 (2011).
[124] Q. H. Fang, H. P. Song, and Y. W. Liu, Misfit dislocations in an annular film grown on a cylindrical nanowire with different elastic constants, Physica B **404**, 1897 (2009).
[125] C. M. Haapamaki, R. R. LaPierre, and J. Baugh, Critical shell thickness for InAs–$Al_xIn_{1-x}As$(P) core–shell nanowires, J. Appl. Phys. **112**, 124305 (2012).
[126] G. E. Cirlin, V. G. Dubrovskii, I. P. Soshnikov, N. V. Sibirev, Y. B. Samsonenko, A. D. Bouravleuv, J. C. Harmand, and F. Glas, Critical diameters and temperature domains for MBE growth of III–V nanowires on lattice mismatched substrates, Phys. Status Solidi RRL **3**, 112 (2009).
[127] E. Ertekin, P. A. Greaney, D. C. Chrzan, and T. D. Sands, Equilibrium limits of coherency in strained nanowire heterostructures, J. Appl. Phys. **97**, 114325 (2005).
[128] H. Ye, P. Lu, Z. Yu, Y. Song, D. Wang, and S. Wang, Critical Thickness and Radius for Axial Heterostructure Nanowires Using Finite-Element Method, Nano Lett. **9**, 1921 (2009).
[129] G. Kastnery and U. Gosele, Stress and dislocations at cross-sectional heterojunctions in a cylindrical nanowire, Philos. Mag. **84**, 3803 (2004).

[130] F. Glas, Critical dimensions for the plastic relaxation of strained axial heterostructures in free-standing nanowires, Phys. Rev. B **74**, 121302 (2006).
[131] K. L. Kavanagh, Misfit dislocations in nanowire heterostructures, Semicond. Sci. Technol. **25**, 024006 (2010).
[132] H. Park, R. Beresford, S. Hong, and J. Xu, Geometry- and size-dependence of electrical properties of metal contacts on semiconducting nanowires, J. Appl. Phys. **108**, 094308 (2010).
[133] H. Ruda and A. Shik, Influence of contacts on the conductivity of thin wires, J. Appl. Phys. **84**, 5867 (1998).
[134] F. Leonard and A. A. Talin, Size-dependent effects on electrical contacts to nanotubes and nanowires, Phys. Rev. Lett. **97**, 026804 (2006).
[135] J. Hu, Y. Liu, C. Z. Ning, R. Dutton, and S.-M. Kang, Fringing field effects on electrical resistivity of semiconductor nanowire-metal contacts, Appl. Phys. Lett. **92**, 083503 (2008).
[136] F. Leonard and A. A. Talin, Electrical contacts to one- and two-dimensional nanomaterials, Nature Nanotechnol. **6**, 773 (2011).
[137] O. Salehzadeh, M. X. Chen, K. L. Kavanagh, and S. P. Watkins, Rectifying characteristics of Te-doped GaAs nanowires, Appl. Phys. Lett. **99**, 182102 (2011).
[138] A. C. E. Chia and R. R. LaPierre, Contact planarization of ensemble nanowires, Nanotechnology **22**, 245304 (2011).
[139] E. Havard, T. Camps, V. Bardinal, L. Salvagnac, C. Armand, C. Fontaine, and S. Pinaud, Effect of thermal annealing on the electrical properties of indium tin oxide (ITO) contact on Be-doped GaAs for optoelectronic applications, Semicond. Sci. Technol. **23**, 035001 (2008).
[140] V. L. Rideout, A review of the theory and technology for Ohmic contacts to group III–V compound semiconductors, Solid-State Electron. **18**, 541 (1975).
[141] M. Heurlin, P. Wickert, S. Falt, M. T. Borgstrom, K. Deppert, L. Samuelson, and M. H. Magnusson, Axial InP nanowire tandem junction grown on a silicon substrate, Nano Lett. **11**, 2028 (2011).
[142] A. Pfund, I. Shorubalko, R. Leturcq, M. T. Borgström, F. Gramm, E. Müller, and K. Ensslin, Fabrication of semiconductor nanowires for electronic transport measurements, Chimia A **726**, 729 (2006).
[143] D. B. Suyatin, C. Thelander, M. T. Bjork, I. Maximov, and L. Samuelson, Sulfur passivation for Ohmic contact formation to InAs nanowires, Nanotechnology **18**, 105307 (2007).
[144] M. Scheffler, S. Nadj-Perge, L. P. Kouwenhoven, M. T. Borgström, and E. P. A. M. Bakkers, Diameter-dependent conductance of InAs nanowires, J. Appl. Phys. **106**, 124303 (2009).
[145] A. C. E. Chia and R. R. LaPierre, Analytical model of surface depletion in GaAs nanowires, J. Appl. Phys. **112**, 063705 (2012).
[146] H. J. Joyce, J. Wong-Leung, C.-K. Yong, C. J. Docherty, S. Paiman, Q. Gao, H. Hoe Tan, C. Jagadish, J. Lloyd-Hughes, L. M. Herz, and M. B. Johnston, Ultralow surface recombination velocity in InP nanowires probed by Terahertz spectroscopy, Nano Lett. **12**, 5325 (2012).
[147] V. N. Bessolov and M. V. Lebedev, Chalcogenide passivation of III–V semiconductor surfaces, Semiconductors **32**, 1141 (1998).
[148] N. Tajik, Z. Peng, P. Kuyanov, and R. R. LaPierre, Sulfur passivation and contact methods in GaAs nanowire solar cells, Nanotechnology **22**, 225402 (2011).
[149] N. Tajik, A. C. E. Chia, and R. R. LaPierre, Improved conductivity and long-term stability of sulfur-passivated n-GaAs nanowires, Appl. Phys. Lett. **100**, 203122 (2012).
[150] O. Demichel, M. Heiss, J. Bleuse, H. Mariette, and A. Fontcuberta i Morral, Impact of surfaces on the optical properties of GaAs nanowires, Appl. Phys. Lett. **97**, 201907 (2010).
[151] P. Parkinson, H. J. Joyce, Q. Gao, H. H. Tan, X. Zhang, J. Zou, C. Jagadish, L. M. Herz, and M. B. Johnston, Carrier lifetime and mobility enhancement in nearly defect-free core−shell nanowires measured using time-resolved Terahertz spectroscopy, Nano Lett. **9**, 3349 (2009).
[152] M. Moewe, L. C. Chuang, S. Crankshaw, C. Chase, and C. Chang-Hasnain, Atomically sharp catalyst-free wurtzite GaAs/AlGaAs nanoneedles grown on silicon, Appl. Phys. Lett. **93**, 023116 (2008).
[153] L. V. Titova, T. B. Hoang, H. E. Jackson, L. M. Smith, J. M. Yarrison-Rice, H. J. Joyce, H. H. Tan, and C. Jagadish, Temperature dependence of photoluminescence from single core-shell GaAs–AlGaAs nanowires, Appl. Phys. Lett. **89**, 173126 (2006).
[154] A. C. E. Chia, M. Tirado, Y. Li, S. Zhao, Z. Mi, D. Comedi, and R. R. LaPierre, Electrical transport and optical model of GaAs–AlInP core–shell nanowires, J. Appl. Phys. **111**, 094319 (2012).
[155] G. Mariani, A. C. Scofield, C.-H. Hung, and D. L. Huffaker, GaAs nanopillar-array solar cells employing in situ surface passivation, Nature Commun. **4**, 1497 (2013).
[156] A. R. Clawson, Guide to references on III–V semiconductor chemical etching, Mater. Sci. Eng. **31**, 1 (2001).
[157] M. Hilse, M. Ramsteiner, S. Breuer, L. Geelhaar, and H. Riechert, Incorporation of the dopants Si and Be into GaAs nanowires, Appl. Phys. Lett. **96**, 193104 (2010).
[158] L. Rigutti, A. De Luna Bugallo, M. Tchernycheva, G. Jacopin, F. H. Julien, G. Cirlin, G. Patriarche, D. Lucot, L. Travers, and J.-C. Harmand, Si incorporation in InP nanowires grown by Au-assisted molecular beam epitaxy, J. Nanomaterials **2009**, 435451 (2009).
[159] J. Dufouleur, C. Colombo, T. Garma, B. Ketterer, E. Uccelli, M. Nicotra, and A. Fontcuberta i Morral, P-doping mechanisms in catalyst-free gallium arsenide nanowires, Nano Lett. **10**, 1734 (2010).
[160] A. Casadei, P. Krogstrup, M. Heiss, J. A. Rohr, C. Colombo, T. Ruelle, S. Upadhyay, C. B. Sorensen, J. Nygard, and A. Fontcuberta i Morral, Doping incorporation paths in catalyst-free Be-doped GaAs nanowires, Appl. Phys. Lett. **102**, 013117 (2013).
[161] E. A. Rienk, M. A. Verheijen, M. T. Borgstrom, L.-F. Feiner, G. Immink, W. J. P. van Enckevort, E. Vlieg, and E. P. A. M. Bakkers, Twinning superlattices in indium phosphide nanowires, Nature **456**, 369 (2008).
[162] J. Wallentin, M. Ek, L. R. Wallenberg, L. Samuelson, K. Deppert, and M. T. Borgstrom, Changes in contact angle of seed particle correlated with increased zincblende formation in doped InP nanowires, Nano Lett. **10**, 4807 (2010).

[163] R. J. Yee, S. J. Gibson, V. G. Dubrovskii, and R. R. LaPierre, Effect of Be doping on InP nanowire growth mechanisms, Appl. Phys. Lett. **101**, 263106 (2012).
[164] J. Wallentin, L. B. Poncela, A. M. Jansson, K. Mergenthaler, M. Ek, D. Jacobsson, L. R. Wallenberg, K. Deppert, L. Samuelson, D. Hessman, and M. T. Borgstrom, Single GaInP nanowire p–i–n junctions near the direct to indirect bandgap crossover point, Appl. Phys. Lett. **100**, 251103 (2012).
[165] J. Wallentin and M. T. Borgström, Doping of semiconductor nanowires, J. Mater. Res. **26**, 2142 (2011).
[166] A. C. E. Chia and R. R. LaPierre, Unlocking doping and compositional profiles of nanowire ensembles using SIMS, Nanotechnology **24**, 045701 (2013).
[167] K. Storm, F. Halvardsson, M. Heurlin, D. Lindgren, A. Gustafsson, P. M. Wu, B. Monemar, and L. Samuelson, Spatially resolved Hall effect measurement in a single semiconductor nanowire, Nature Nanotechnol. **7**, 718 (2012).
[168] Ch. Blömers, T. Grap, M. I. Lepsa, J. Moers, St. Trellenkamp, D. Grützmacher, H. Lüth, and T. Schäpers, Hall effect measurements on InAs nanowires, Appl. Phys. Lett. **101**, 152106 (2012).
[169] D. E. Perea, E. R. Hemesath, E. J. Schwalbach, J. L. Lensch-Falk, P. W. Voorhees, and L. J. Lauhon, Direct measurement of dopant distribution in an individual vapour–liquid–solid nanowire, Nature Nanotechnol. **4**, 315 (2009).
[170] J. D. Christesen, X. Zhang, C. W. Pinion, T. A. Celano, C. J. Flynn, and J. F. Cahoon, Design principles for photovoltaic devices based on Si nanowires with axial or radial p−n junctions, Nano Lett. **12**, 6024 (2012).
[171] A. Kandala, T. Betti, and A. Fontcuberta i Morral, General theoretical considerations on nanowire solar cell designs, Phys. Status Solidi A **206**, 173 (2009).
[172] A. D. Mallorquı, F. M. Epple, D. Fan, O. Demichel, and A. Fontcuberta i Morral, Effect of the pn junction engineering on Si microwire-array solar cells, Phys. Status Solidi A **209**, 1588 (2012).
[173] S. Bu, X. Li, L. Wen, X. Zeng, Y. Zhao, W. Wang, and Y. Wang, Optical and electrical simulations of two-junction III–V nanowires on Si solar cell, Appl. Phys. Lett. **102**, 031106 (2013).
[174] I. Vurgaftman, J. R. Meyer, and L. R. Ram-Mohan, Band parameters for III–V compound semiconductors and their alloys, J. Appl. Phys. **89**, 5815 (2001).
[175] T. Mårtensson, C. P. T. Svensson, B. Wacaser, M. W. Larsson, W. Seifert, K. Deppert, A. Gustafsson, L. R. Wallenberg, and L. Samuelson, Epitaxial III–V nanowires on silicon, Nano Lett. **4**, 1987 (2004).
[176] P. K. Mohseni, C. Maunders, G. A. Botton, and R. R. LaPierre, GaP/GaAsP/GaP core-multishell nanowire heterostructures on (111) silicon, Nanotechnology **18**, 445304 (2007).
[177] P. K. Mohseni, A. D. Rodrigues, J. C. Galzerani, Y. A. Pusep, and R. R. LaPierre, Structural and optical analysis of GaAsP/GaP core-shell nanowires, J. Appl. Phys. **106**, 124306 (2009).
[178] A. Fakhr, Y. M. Haddara, and R. R. LaPierre, Dependence of InGaP nanowire morphology and structure on molecular beam epitaxy growth conditions, Nanotechnology **21**, 165601 (2010).
[179] D. Jacobsson, J. M. Persson, D. Kriegner, T. Etzelstorfer, J. Wallentin, J. B. Wagner, J. Stangl, L. Samuelson, K. Deppert, and M. T. Borgstrom, Particle-assisted $Ga_xIn_{1-x}P$ nanowire growth for designed bandgap structures, Nanotechnology **23**, 245601 (2012).
[180] J. Wallentin, L. B. Poncela, A. M. Jansson, K. Mergenthaler, M. Ek, D. Jacobsson, L. R. Wallenberg, K. Deppert, L. Samuelson, D. Hessman, and M. T. Borgstrom, Single GaInP nanowire p–i–n junctions near the direct to indirect bandgap crossover point, Appl. Phys. Lett. **100**, 251103 (2012).
[181] M. Tchernycheva, L. Rigutti, G. Jacopin, A. de Luna Bugallo, P. Lavenus, F. H. Julien, M. Timofeeva, A. D. Bouravleuv, G. E. Cirlin, V. Dhaka, H. Lipsanen, and L. Largeau, Photovoltaic properties of GaAsP core–shell nanowires on Si(001) substrate, Nanotechnology **23**, 265402 (2012).
[182] Y. Hu, M. Li, J.-J. He, and R. R. LaPierre, Current matching and efficiency optimization in a two-junction nanowire-on-silicon solar cell, Nanotechnology **24**, 065402 (2013).
[183] J. Wallentin, J. M. Persson, J. B. Wagner, L. Samuelson, K. Deppert, and M. T. Borgstrom, High-performance single nanowire tunnel diodes, Nano Lett. **10**, 974 (2010).
[184] B. M. Borg, K. A. Dick, B. Ganjipour, M.-E. Pistol, L.-E. Wernersson, and C. Thelander, InAs/GaSb heterostructure nanowires for tunnel field-effect transistors, Nano Lett. **10**, 4080 (2010).
[185] B. Ganjipour, A. W. Dey, B. M. Borg, M. Ek, M.-E. Pistol, K. A. Dick, L.-E. Wernersson, and C. Thelander, High current density Esaki tunnel diodes based on GaSb–InAsSb heterostructure nanowires, Nano Lett. **11**, 4222 (2011).
[186] J. Yang, J. Goguen, and R. Kleiman, Silicon solar cell with integrated tunnel junction for multi-junction photovoltaic applications, IEEE Electron Device Lett. **33**, 1732 (2012).
[187] L. Wen, X. Li, Z. Zhao, S. Bu, X. Zeng, J. Huang, and Y. Wang, Theoretical consideration of III–V nanowire/Si triple-junction solar cells, Nanotechnology **23**, 505202 (2012).
[188] K. A. Dick, K. Deppert, L. S. Karlsson, L. R. Wallenberg, L. Samuelson, and W. Seifert, A new understanding of Au-assisted growth of III–V semiconductor nanowires, Adv. Funct. Mater. **15**, 1603 (2005).
[189] K. A. Dick, S. Kodambaka, M. C. Reuter, K. Deppert, L. Samuelson, W. Seifert, L. R. Wallenberg, and F. M. Ross, The morphology of axial and branched nanowire heterostructures, Nano Lett. **7**, 1817 (2007).
[190] K. A. Dick, J. Bolinsson, B. M. Borg, and J. Johansson, Controlling the abruptness of axial heterojunctions in III–V nanowires: Beyond the reservoir effect, Nano Lett. **12**, 3200 (2012).
[191] J. A. Czaban, D. A. Thompson, and R. R. LaPierre, GaAs core–shell nanowires for photovoltaic applications, Nano Lett. **9**, 148 (2009).
[192] H. Bi and R. R. LaPierre, A GaAs nanowire-P3HT hybrid photovoltaic device, Nanotechnology **20**, 465205 (2009).
[193] G. Mariani, R. B. Laghumavarapu, B. Tremolet de Villers, J. Shapiro, P. Senanayake, A. Lin, B. J. Schwartz, and

D. L. Huffaker, Hybrid conjugated polymer solar cells using patterned GaAs nanopillars, Appl. Phys. Lett. **97**, 013107 (2010).

[194] G. E. Cirlin, A. D. Bouravleuv, I. P. Soshnikov, Yu. B. Samsonenko, V. G. Dubrovskii, E. M. Arakcheeva, E. M. Tanklevskaya, and P. Werner, Photovoltaic properties of p-doped GaAs nanowire arrays grown on n-type GaAs(111)B substrate, Nanoscale Res. Lett. **5**, 360 (2010).

[195] G. Mariani, P.-S. Wong, A. M. Katzenmeyer, F. Leonard, J. Shapiro, and D. L. Huffaker, Patterned radial GaAs nanopillar solar cells, Nano Lett. **11**, 2490 (2011).

[196] N. Han, F. Wang, S. Yip, J. J. Hou, F. Xiu, X. Shi, A. T. Hui, T. Hung, and J. C. Ho, GaAs nanowire Schottky barrier photovoltaics utilizing Au–Ga alloy catalytic tips, Appl. Phys. Lett. **101**, 013105 (2012).

[197] C. Colombo, M. Heiss, M. Gratzel, and A. Fontcuberta i Morral, Gallium arsenide p–i–n radial structures for photovoltaic applications, Appl. Phys. Lett. **94**, 173108 (2009).

[198] J.-J. Chao, S.-C. Shiu, and C.-F. Lin, GaAs nanowire/poly(3,4ethylenedioxythiophene):poly(styrenesulfonate) hybrid solar cells with incorporating electron blocking poly(3-hexylthiophene) layer, Sol. Energy Mater. Sol. Cells **105**, 40 (2012).

[199] W. Wei, X.-Y. Bao, C. Soci, Y. Ding, Z.-L. Wang, and D. Wang, Direct heteroepitaxy of vertical InAs nanowires on Si substrates for broad band photovoltaics and photodetection, Nano Lett. **9**, 2926 (2009).

[200] C. J. Novotny, E. T. Yu, and P. K. L. Yu, InP nanowire/polymer hybrid photodiode, Nano Lett. **8**, 775 (2008).

[201] H. Goto, K. Nosaki, K. Tomioka, S. Hara, K. Hiruma, J. Motohisa, and T. Fukui, Growth of core–shell InP nanowires for photovoltaic application by selective-area metal organic vapor phase epitaxy, Appl. Phys. Express **2**, 035004 (2009).

[202] J. Wallentin, N. Anttu, D. Asoli, M. Huffman, I. Åberg, M. H. Magnusson, G. Siefer, P. Fuss-Kailuweit, F. Dimroth, B. Witzigmann, H. Q. Xu, L. Samuelson, K. Deppert, and M. T. Borgström, InP nanowire array solar cells achieving 13.8% efficiency by exceeding the ray optics limit, Science **339**, 1057 (2013).

[203] H. Pham, T. Nguyen, Y.-L. Chang, I. Shih, and Z. Mi, InN p–i–n nanowire solar cells on Si, IEEE J. Sel. Top. Quantum Electron. **17**, 1062 (2011).

[204] Y. B. Tang, Z. H. Chen, H. S. Song, C. S. Lee, H. T. Cong, H. M. Cheng, W. J. Zhang, I. Bello, and S. T. Lee, Vertically aligned p-type single-crystalline GaN nanorod arrays on n-Type Si for heterojunction photovoltaic cells, Nano Lett. **8**, 4191 (2008).

[205] Y. Dong, B. Tian, T. J. Kempa, and C. M. Lieber, Coaxial group III-nitride nanowire photovoltaics, Nano Lett. **9**, 2183 (2009).

[206] J. C. Shin, K. H. Kim, K. J. Yu, H. Hu, L. Yin, C.-Z. Ning, J. A. Rogers, J.-M. Zuo, and X. Li, $In_xGa_{1-x}As$ nanowires on silicon: One-dimensional heterogeneous epitaxy, bandgap engineering, and photovoltaics, Nano Lett. **11**, 4831 (2011).

[207] C. Gutsche, A. Lysov, D. Braam, I. Regolin, G. Keller, Z.-A. Li, M. Geller, M. Spasova, W. Prost, and F.-J. Tegude, n-GaAs/InGaP/p-GaAs core-multishell nanowire diodes for efficient light-to-current conversion, Adv. Funct. Mater. **22**, 929 (2012).

[208] M. Tchernycheva, L. Rigutti, G. Jacopin, A. de Luna Bugallo, P. Lavenus, F. H. Julien, M. Timofeeva, A. D. Bouravleuv, G. E. Cirlin, V. Dhaka, H. Lipsanen, and L. Largeau, Photovoltaic properties of GaAsP core–shell nanowires on Si(001) substrate, Nanotechnology **23**, 265402 (2012).

[209] J. V. Holm, H. I. Jørgensen, P. Krogstrup, J. Nygård, H. Liu, and M. Aagesen, Surface-passivated GaAsP single-nanowire solar cells exceeding 10% efficiency grown on silicon, Nature Commun. **4**, 1498 (2013).

[210] T. J. Kempa, B. Tian, D. R. Kim, J. Hu, X. Zheng, and C. M. Lieber, Single and tandem axial p–i–n nanowire photovoltaic devices, Nano Lett. **8**, 3456 (2008).

[211] P. K. Mohseni, A. Behnam, J. D. Wood, C. D. English, J. W. Lyding, E. Pop, and X. Li, $In_xGa_{1-x}As$ nanowire growth on graphene: van der Waals epitaxy induced phase segregation, Nano Lett. **13**, 1153 (2013).

[212] A. M. Munshi, D. L. Dheeraj, V. T. Fauske, D.-C. Kim, A. T. J. van Helvoort, B.-O. Fimland, and H. Weman, Vertically aligned GaAs nanowires on graphite and few-layer graphene: generic model and epitaxial growth, Nano Lett. **12**, 4570 (2012).

[213] P. K. Mohseni, G. Lawson, A. Adronov, and R. R. LaPierre, Hybrid GaAs nanowire-carbon nanotube flexible photovoltaics, IEEE J. Sel. Top. Quantum Electron. **17**, 1070 (2011).

[214] P. K. Mohseni, G. Lawson, C. Couteau, G. Weihs, A. Adronov, and R. R. LaPierre, Growth and characterization of GaAs nanowires on carbon nanotube composite films: towards flexible nano-devices, Nano Lett. **8**, 4075 (2008).

[215] Y. J. Hong, W. H. Lee, Y. Wu, R. S. Ruoff, and T. Fukui, van der Waals epitaxy of InAs nanowires vertically aligned on single-layer graphene, Nano Lett. **12**, 1431 (2012).

[216] J. M. Spurgeon, S. W. Boettcher, M. D. Kelzenberg, B. S. Brunschwig, H. A. Atwater, and N. S. Lewis, Flexible, polymer-supported, Si wire array photoelectrodes, Adv. Mater. **22**, 3277 (2010).

[217] Y. G. Sun and J. A. Rogers, Fabricating semiconductor nano/microwires and transfer printing ordered arrays of them onto plastic substrates, Nano Lett. **4**, 1953 (2004).

[218] A. J. Standing, S. Assali, J. E. M. Haverkort, and E. P. A. M. Bakkers, High yield transfer of ordered nanowire arrays into transparent flexible polymer films, Nanotechnology **23**, 495305 (2012).

[219] M. Heurlin, M. H. Magnusson, D. Lindgren, M. Ek, L. R. Wallenberg, K. Deppert, and L. Samuelson, Continuous gas-phase synthesis of nanowires with tunable properties, Nature **492**, 90 (2013).

